

MODES OF INTER-ANNUAL VARIABILITY OF ATMOSPHERIC MOISTURE FLUX TRANSPORT

Francina Dominguez*, Praveen Kumar
Department of Civil and Environmental Engineering
University of Illinois at Urbana-Champaign

1. INTRODUCTION

Large-scale circulation patterns, as well as local recycling, are the main mechanisms of moisture transport in the atmosphere. By evaluating the relative contribution of these mechanisms in the hydrology of a region, we will gain a better understanding of the physical processes responsible for inter-annual variability in the hydrologic cycle. To this end we need to understand the principal modes of moisture flux transport in the atmosphere. In order to obtain the modes of moisture transport, rotated principal component analysis (RPCA) is performed on the magnitudes of moisture flux for each season obtained from the 54-year Reanalysis I data. The stability of these predominant modes is evaluated by partitioning the analysis data in two 27-year periods, and obtaining the predominant modes for these sub-sets of the data. The modes that appear in both of the first and second periods, as well as in the entire data set are said to be stable. The stable modes that account for the greatest variability in the data are compared and related to large-

scale circulation patterns such as the Artic Oscillation (AO), the North Atlantic Oscillation (NAO) and Pacific North American Pattern (PNA), which have been well established in the literature. The discussion that follows will concentrate mostly on the analysis of the winter season, as an example of the methodology that is being used for all the four seasons.

2. DATA AND INTEGRATION

The 6-hourly NCEP/NCAR Reanalysis I data provides 54 complete years of meteorological variables. The reliability and shortcomings of the NCEP/NCAR reanalysis data have been previously studied. *Higgins et al.* [1996], *Mo and Higgings* [1996], and *Higgins and Mo* [1996] compared the moisture budget and moisture transport captured by the NCEP/NCAR and NASA/DAO reanalyses.

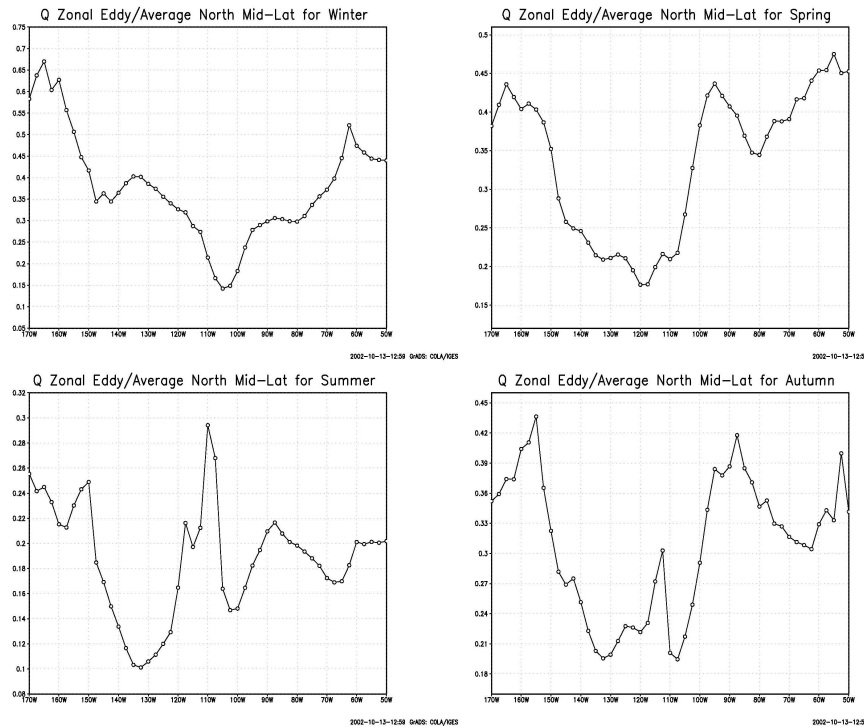


Figure 1 Eddy/Average is the magnitude of the eddy flux divided by the magnitude of the average flux, averaged over the 54 year period between 30°N and 60°N. The diagram shows this value between 170° W and 50° W.

They found that the NCEP/NCAR reanalysis significantly overestimated precipitation, but did a good job of capturing precipitation events over the Great Plains. *Higgins et al.* [1997] examined the quality of the NCEP/NCAR and NASA/DAO reanalysis wind fields by comparing them to observations and using them to identify low-level jet (LLJ). The NCEP/NCAR reanalysis was found to do a reasonable job of capturing some of the vertical characteristics of the Great Plains LLJ. The resolution of the Reanalysis Model is T62 (209 km) with 28 vertical sigma levels. The output has been converted to a 2.5 by 2.5 degree lat-lon grid, while keeping all the 28 levels in order to get a higher resolution close to the surface. Zonal and meridional moisture fluxes are integrated over the entire atmospheric column and the seasonal average and seasonal eddy fluxes are obtained for the whole period.

$$Q_x = \int_{p_s}^{p_t} \overline{qu} \frac{dp}{g} + \int_{p_s}^{p_t} \overline{q'u'} \frac{dp}{g} \quad (1)$$

$$Q_y = \int_{p_s}^{p_t} \overline{qv} \frac{dp}{g} + \int_{p_s}^{p_t} \overline{q'v'} \frac{dp}{g} \quad (2)$$

Qx = total zonal moisture flux
 Qy = total meridional moisture flux
 q = specific humidity
 u, v = zonal and meridional wind
 ps = surface pressure
 pt = 0.0027 * ps

The importance of including the eddy fluxes in the analysis can be seen in Figure 1. In mid-latitudes the eddy flux over the average flux has a maximum value of 67% in winter, and often reaches values of over 40% during spring and autumn.

3. ROTATED PRINCIPAL COMPONENT ANALYSIS (RPCA)

RPCA has been extensively used in atmospheric studies. In this work, we perform RPCA on the integrated water vapor flux magnitudes over North America (170 – 50°W and 10 – 80°N). The data matrix has 1421 columns (each column corresponding to a grid box in the analysis domain) and 54 rows (number of years of data), corresponding to the S mode of analysis of the six modes summarized by *Richman* [1986]. The correlation matrix rather than the covariance matrix is used to evaluate the principal component so that variations in the data are standardized at each sample point. The first 15 components are then orthogonally rotated using a varimax rotation. Figure 2 shows the cumulative variance represented by each rotated mode for winter, we can see that the first 15 modes account for 85.1% of the variation in the data, this means that the rotation of more than 15 modes will not result in the addition of any more significant modes of variability. The first and second modes account for 8.7% of variation respectively, followed by 8.6% explained by the third mode.

According to *Richman* (1985), the RPCA analysis is superior to PCA when analyzing individual modes of variation in data analysis. The RPCA will enable us to achieve a simpler structure than that for PCA, and this is helpful when physically interpreting the data. Figure 3 shows biplots the first two winter modes (x and y axis) before and after rotation. The rotated biplot shows that there is a clustering of elements along the zero axes, resulting in fewer outlying points in the figures. This produces PCs that are easily interpreted

Percentage of Variance explained by rotated components Totwinte

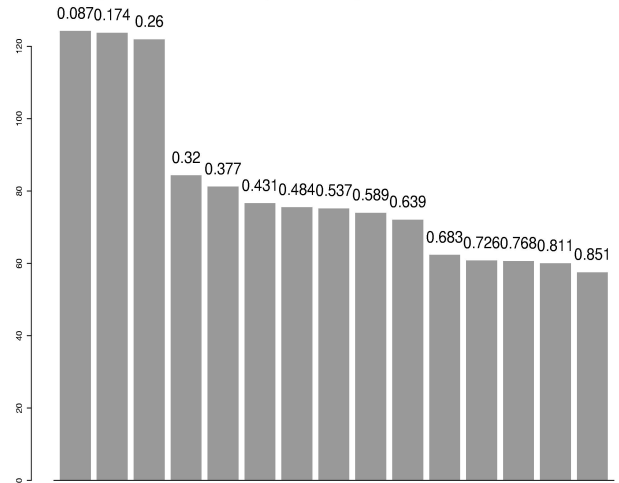
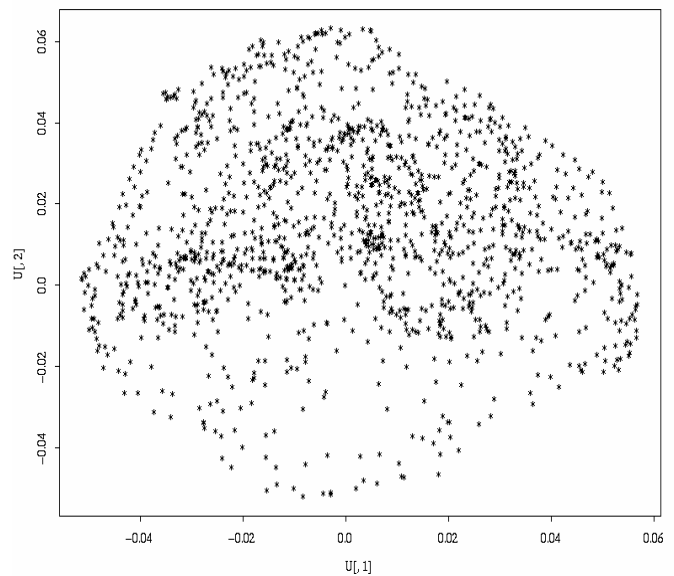


Figure 2 Total variance and cumulative variance explained by the first 15 components for Winter.



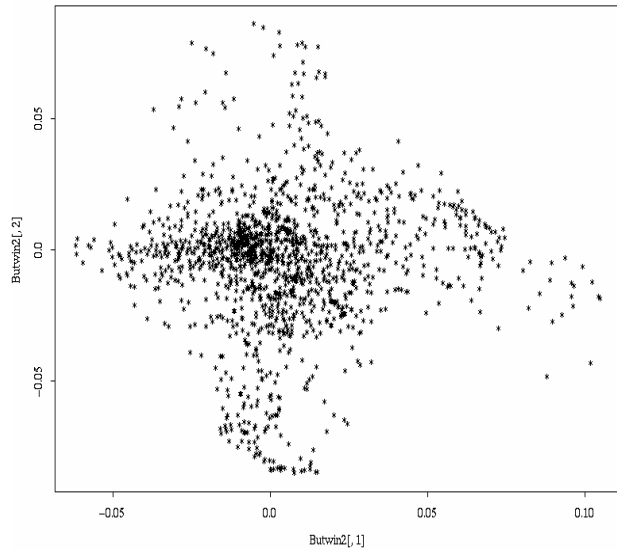


Figure 3 Biplots of the first two winter components before and after orthogonal varimax rotation.

The discussion that follows will concentrate on the first two winter components in order to illustrate the methodology used for the interpretation of all of the seasonal modes of variation.

RESULTS

Weighted scores for the rotated principal components are obtained by multiplying the rotated eigenvectors by a scaled matrix of the original data. This scaling is accomplished by subtracting the mean of each column of the data matrix and then dividing each column by the square root of the corresponding diagonal element of the covariance matrix of the data.

For the most dominant components, mean subtracted values of the flux ($Q - \overline{Q}$) are averaged for (1) all years that have a score above one standard deviation, and (2) all years that have a score below one standard deviation. These are identified as positive and negative phases of the same mode.

Figure 4 shows the scores of the first two winter components.

Figure 5 shows the positive and negative phases of the first winter mode. A dashed line encloses the analysis domain (10°N to 80°N and 170°W to 50°W), however, the spatial patterns are presented for an expanded domain to facilitate identification of broader circulation patterns and climatological conditions contributing to each mode. As we can clearly see, the positive and negative phases of the mode show the same pattern but

with opposing signs. Two distinct areas of influence are visible (1) three bands of alternating sign extending from 100°W to 0° and 10°N to 50°N (2) A band in the Pacific Ocean extending from 180°W to 120°W with a center around 30°N, and a smaller band of opposing sign directly to the north.

Figure 5 shows the positive and negative phases of the second mode. This mode is characterized by a band extending from the Pacific Ocean (180°W, around 30°N) then flowing north at around 145°W, and reaching the continent at around 60°N.

The positive and negative phases of the anomalies of the 500mb geopotential height are obtained in a similar way as the flux anomalies. The positive and negative phases are obtained by averaging the geopotential height anomalies for the same years as the moisture flux data. The $Qu - \overline{Qu}$, $Qv - \overline{Qv}$ moisture flux vector field is then plotted over the geopotential height field in order to compare the two fields, and determine the influence that the large-scale geopotential height anomalies have on the modes of moisture transport.

Figure 6 shows the geopotential heights corresponding to the same years as the first winter mode of moisture flux. The most dominant feature is a band extending from around 35°N to 60°N and 180°W to 120°W, a band of the same sign over the southeastern United States (110°W to 40°W with a center around 30°N) and a very large band of opposite sign over Canada, and part of the northern United States. The moisture flux vector field closely follows the patterns in the geopotential height. This leads us to believe that the first mode of winter transport is dominated by these large-scale patterns.

The geopotential height anomalies corresponding to the second mode are characterized by two centers of opposing sign over the Pacific Ocean and northwestern North American Continent, as seen in Figure 6. These two bands of opposing signs are located around 40°N and 60°N with the centers of opposing sign at 170°W and 130°W. The moisture flux vector field closely follows the geopotential height anomaly fields, as was the case with the first mode of moisture transport. This geopotential height pattern presents the most dominant features of the Pacific/North American Pattern (PNA) which has been extensively discussed in previous studies *Barnston and Livezey* (1986).

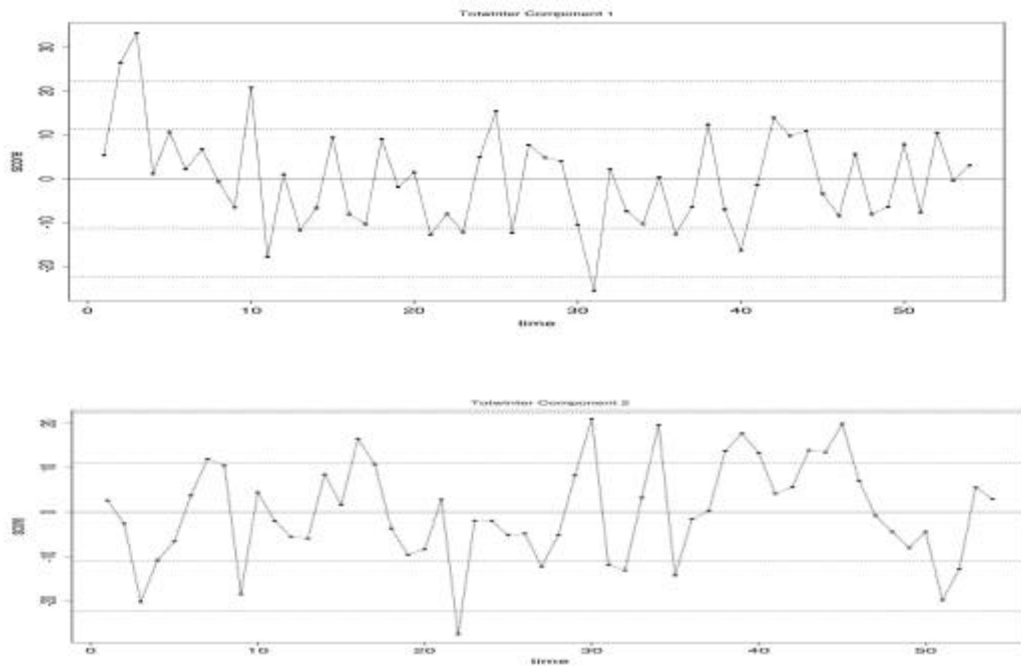


Figure 4 Scores for the first two components for winter. Including the one and two standard deviation lines. In the x axis, 0 corresponds to 1948 and 50 corresponds to 1998

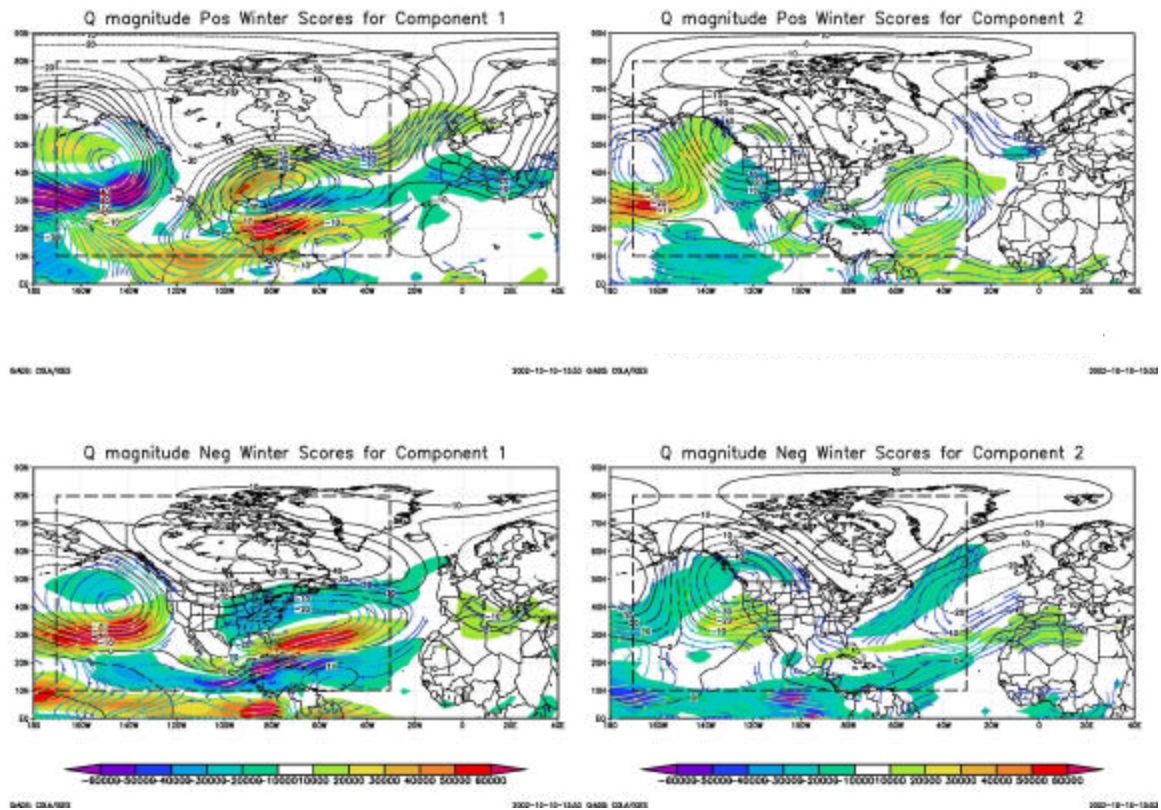


Figure 5 Mean subtracted moisture flux magnitude ($Q - \bar{Q}$) corresponding to the positive and negative phases of the first winter mode (left), and second winter mode(right).

4. STABILITY

The robustness of the modes was tested by evaluating the sensitivity of the results to a reduction in the period of analysis. The 54-year period was partitioned into two 27-year subsets and the above methodology was replicated separately for each of the data sets. If a mode that had been identified using the whole period was clearly presented in the two 27-year subsets, the mode was said to be stable. If it was only clearly seen in one of the subsets the mode was said to be partially stable. Table 1 shows the results for the first six winter modes. As we can see, the first three winter modes are stable, while the other three only appear in one of the sub-sets of the data.

Winter Mode	1948-1974 data set Mode	1975-2001 data set mode	Stability Analysis
1	1	1	Stable
2	5	2	Stable
3	6	3	Stable
4	3		P-Stable
5	4		P-Stable
6		6	P-Stable

Table 1 Stability analysis of the first six winter modes. The modes in the sub-sets that present the same pattern as the original winter modes are presented in columns 2 and 3. Column 4 determines the stability.

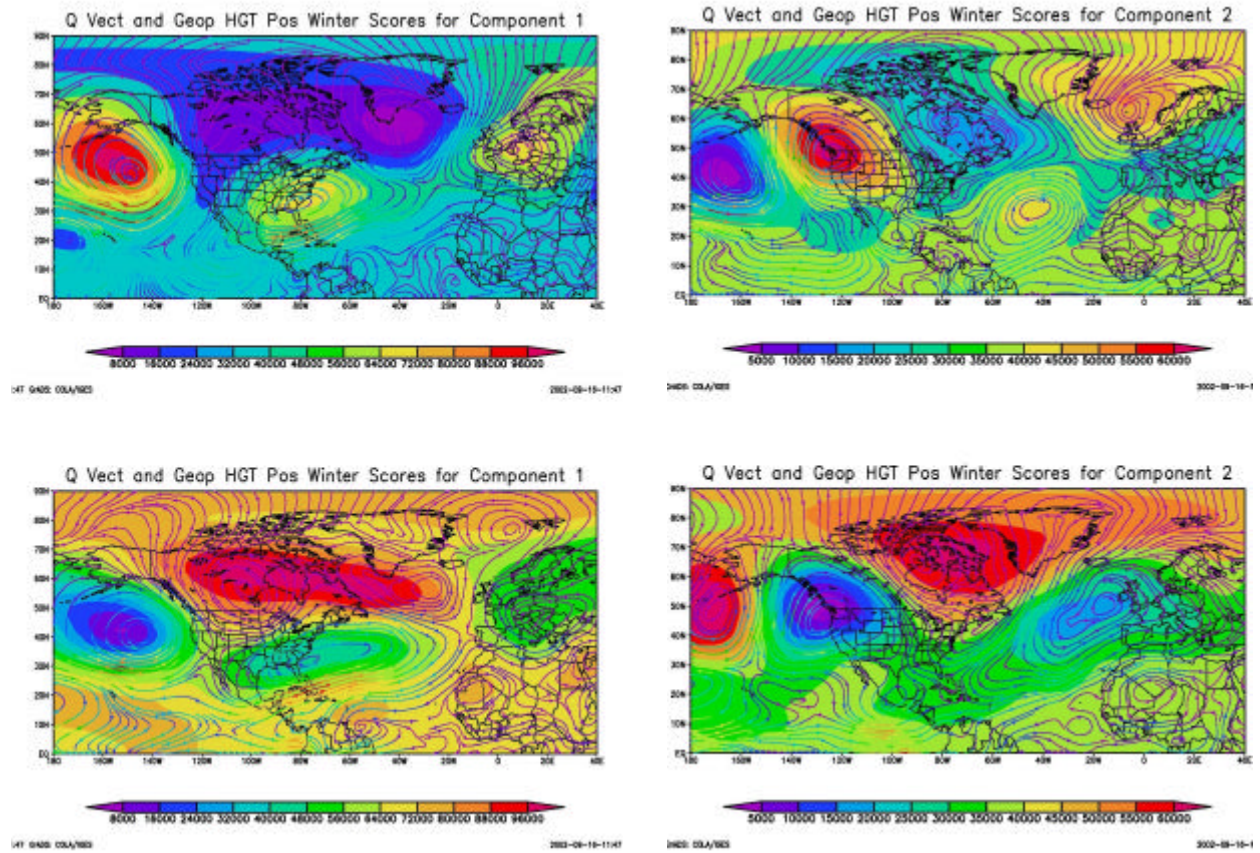


Figure 6 Mean subtracted geopotential height ($\overline{hgt} - \overline{hgt}$) corresponding to the positive and negative phases of the first winter mode, overlaid by the corresponding mean subtracted water vapor flux field.

CONCLUSIONS

We are currently evaluating all of the seasons with the same methodology we have discussed above for the winter season. The results we have obtained show that RPCA gives us a tool to identify the most important mechanisms of moisture transport in the atmosphere and to better understand the physical processes responsible for inter-annual variability in the hydrologic cycle. For the two modes shown in the winter season, the moisture flux fields have been directly linked to large-scale geopotential height anomalies. This is not the case for all of the modes. Our hypothesis is that local recycling is the driving force behind the modes that cannot be related to large-scale circulation patterns, at least in summer. The hydrology of a region is greatly influenced by the relative contribution of these two mechanisms of moisture transport. The aim of this research is to quantify these contributions for the various modes of moisture transport. This will be an important step in understanding the fundamental interaction between the atmospheric and terrestrial branches of the hydrologic cycle. It will also help us understand the inter-annual variability observed in water bodies such as rivers and lakes, due to atmospheric moisture flux variations.

REFERENCES

- Barnston, Anthony G., and Robert E. Livezey, 1987: Classification, Seasonality and Persistence of Low-Frequency Atmospheric Circulation Patterns. *Monthly Weather Review*, Vol 115, pp. 1083-1126.
- Higgins, R.W., K. C. Mo, and S. D. Schubert, 1996: The Moisture Budget of the Central United States in Spring as Evaluated in the NCEP/NCAR and NASA/DAO Reanalysis, *Monthly Weather Review*, Vol. 124, pp. 939-963.
- Higgins, R. W., and K. C. Mo, 1996: The Moisture Budget of the Central United States as Evaluated in the NCEP/NCAR and NASA/DAO Reanalysis, *Journal of Climate*, Vol. 9, pp. 1531-1545
- Higgins, R.W., Y. Yao, E.S. Yarosh, J.E. Janowiak, and K. C. Mo, 1997: Influence of the Great Plains Low-Level Jet on Summertime Precipitation and Moisture Transport over the Central United States.
- Mo, K. C., and R. W. Higgins, 1996: The Climate Signal in Regional Moisture Fluxes: A Comparison of Three Global Data Assimilation Products, *Journal of Climate*, Vol. 9, pp 1531-1545.
- Richman, Michael B., 1986: Review Article, Rotation of Principal Components, *Journal of Climatology*, Vol. 6, pp. 293-335.